17th Brazilian Congress of Thermal Sciences and Engineering
November 25th-28th, 2018, Águas de Lindóia, SP, Brazil

EFFECTS OF POROSITY AND MEAN PARTICLE DIAMETER ON PERFORMANCE OF A SOLAR VOLUMETRIC RECEIVER

Roberta R. Ribeiro*
Marcelo J.S. de Lemos
Departamento de Energia - IEME
Instituto Tecnológico de Aeronáutica - ITA
12228-900 – São José dos Campos – S.P. Brazil
*Corresponding authors, email: robertadosreisribeiro@gmail.com.

Abstract. This work presents numerical results of the investigation of the thermal performance of a volumetric solar receiver. The Thermal Non-Equilibrium Model and Rosseland approximation are utilized. The numerical technique employed for discretizing the governing equations was the control volume method with a boundary-fitted non-orthogonal coordinate system. The SIMPLE algorithm was used to handle the pressure-velocity coupling. Effects of porosity (ϕ) and mean particle diameter (D_p) in the solid-fluid temperature distributions and pressure drop on absorber porous were investigated. These solutions can serve as a useful tool in the preliminary design of a volumetric solar receiver.

Keywords: *Thermal Non-equilibrium, Solar Volumetric Receiver, Porous Media, Radiation*

1. INTRODUCTION

Solar energy, considered as a source of renewable energy and of abundant nature, presents itself as an interesting option in the generation of electric energy (Kreider and kreith, 1982). Thus, at present there are several technologies of solar concentrators of power (Concentrating Solar Power - CSP). Among the most promising ones, we can highlight the Central Receiver System (CRS) (Omar *et al.*, 2013). However, more research and development (R & D) should be undertaken to reduce costs associated with innovation technology in subsystems or components, and also to consolidate itself as one of the best choices among existing CSP technologies (Roldán *et al.*, 2016).

Solar Receiver (SR) is one of the main components of a CRS that can represent 15% of the total investment cost of a CRS plant (Liao et al., 2014). The SR can be classified, mainly according to their geometric configuration, type of material of the absorber (metallic or ceramic), among others (Hendricks and Howell,1996; Kuwahara *et al.*, 2001; Aichmayer.; 2011; Hoffschmidt.et al, 2003; Félix, 2003; Heller et al. 2006). The Solar Receiver Volumetric (SRV) is a type of SR, usually located at the top of a tower of the CRS, which takes advantage of solar radiation concentrated at high temperatures, generated from a system or set of mirrors or heliostats.

In the literature, we find several analytical, experimental and numerical investigations about the thermal and hydrodynamic behavior of SRV. Fend *et al.* (2004) measured the pressure drop in MH, obtaining linear behavior, due to the strong viscous predominance, characteristic results frequently observed in MH structures Wu *et al.* (2010) and Wu *et al.* (2011) carried out a series of experimental works on SIC OCF absorbers, in order to obtain characteristic curves of the pressure drop as a function of pore diameter and / or porosity.

Mathematical model

The mathematical model here employed has been already fully described in the open literature. It is here extended to simulate radiation, laminar convection flow in a model Solar Receiver Volumetric. As the macroscopic model is already available elsewhere (De Lemos, M., 2012), governing Equations will be just presented and are summarized as follows:

Mass continuity

The macroscopic mass continuity for an incompressible fluid flowing through a porous medium, such as is given by,

$$\nabla \cdot \overline{\mathbf{u}}_D = 0 \tag{1}$$

where $\overline{\mathbf{u}}_D$ is the average surface velocity (also known as seepage, superficial or Darcy Velocity).

Momentum Equation

The Equation (2) shows, the macroscopic momentum Equation (Navier-Stokes) for an incompressible fluid with constant properties flowing through a porous medium can be written as:

$$\nabla \cdot \left(\rho_f \frac{\overline{\mathbf{u}}_D \overline{\mathbf{u}}_D}{\phi} \right) = -\nabla\left(\phi \langle \overline{p} \rangle^i\right) + \mu \nabla^2 \overline{\mathbf{u}}_D + \nabla \cdot \left(-\rho_f \phi \langle \overline{\mathbf{u}' \mathbf{u}'} \rangle^i \right) - \left[\frac{\mu \phi}{K} \overline{\mathbf{u}}_D + \frac{c_F \phi \rho_f |\overline{\mathbf{u}}_D| \overline{\mathbf{u}}_D}{\sqrt{K}} \right] \tag{2}$$

where the last two terms in Equation (2) represent the Darcy and Forchheimer contributions. The symbol K is the porous medium permeability, $c_F = 0.55$ is the form drag coefficient, $\langle p \rangle^i$ is the intrinsic average pressure of the fluid phase, μ represents the fluid viscosity and ϕ is the porosity of the porous medium. The permeability K of the porous matrix is determined using the Equation (3),

$$K = \frac{\phi^3 D^2}{144(1-\phi)} \tag{3}$$

Two-Energy Equation Model

When average temperatures in distinct phases are substantially different from each other, for example in solar receiver device, energy storage units, combustion processes, etc. Macroscopic energy equations are obtained for both fluid and solid phases by applying time and volume average operators to the instantaneous local Equations (4) we name this approach Local Thermal Non Equilibrium (LTNE). After including the fluid and the solid phase energy balance (5). One gets the following Equations:

Fluid: $$\nabla \cdot (\rho_f \, c_{pf} \, \mathbf{u}_D \langle \overline{T_f} \rangle^i) = \nabla \cdot \left\{ \mathbf{K}_{eff,f} \cdot \nabla \langle \overline{T}_f \rangle^i \right\} + h_i a_i \left(\langle \overline{T_s} \rangle^i - \langle \overline{T_f} \rangle^i \right) \tag{4}$$

Solid: $$0 = \nabla \cdot \left\{ \mathbf{K}_{eff,s} \cdot \nabla \langle \overline{T_s} \rangle^i \right\} - h_i a_i \left(\langle \overline{T_s} \rangle^i - \langle \overline{T_f} \rangle^i \right) \tag{5}$$

where, $a_i = A_i / \Delta V$ is the interfacial area per unit volume, h_i is the film coefficient for interfacial transport, $\mathbf{K}_{eff,f}$ and $\mathbf{K}_{eff,s}$ are the effective conductivity tensors for fluid and solid.

Discretization

In the present simulation, the solar volumetric receiver It was represented by a scheme, as shown in the Figure 1*a*. The above Equation set was discretized for a two-dimensional computational domain using the discretization molecule shown in Figure 1*b*. A hybrid numerical scheme was used for interpolating the convection fluxes. The interpolated schemes are Upwind Differencing Scheme (UDS) and Central Differencing Scheme (CDS). The SIMPLE algorithm proposed by **Erro! Fonte de referência não encontrada.** is applied for handling the pressure-velocity coupling.

The discretization form for a two-dimensional conservation Equation of a generic property φ in steady-state regime is as follows,

$$I_e + I_w + I_n + I_s = S_\varphi \tag{6}$$

In Equation (6), the variables I_e, I_w, I_n, and I_s represent the fluxes of φ in the faces east, west, north and south, respectively, and S_φ is the source term.

Standard source term linearization was accomplished by using the following Equation,

$$S_\varphi \approx S_\varphi^{**}\phi_P\langle\varphi\rangle_P^i + S_\varphi^* \tag{7}$$

where ϕ_P is the porosity of node *P*.

For the momentum Equation, discretization in the *x*-direction gives,

$$S^{*x} = (S_e^{*x})_p - (S_w^{*x}) + (S_n^{*x})_p - (S_s^{*x}) + S_p^* \tag{8}$$

$$S^{**x} = S_\varphi^{**} \tag{9}$$

In Equation (10) the term S^{*x} is part of the diffusion fluxes that was treated in an explicit form in addition to the pressure term. The term S^{**x} in Equation (11) entails the additional drag forces due to the porous matrix, last two terms in Equation (2), which are here treated implicitly.

Algebraic Equation sets for all variables were solved by the SIP procedure of Stone (1968). In all computations presented in this work the normalized residues of all transport equations involved were brought down to 1×10^{-9} before convergence was assumed to be achieved.

Radiation boundary condition

At inlet of the absorber, as depicted in Figure 1*c*, the radiation inlet was assumed to be equal the conduction flux reaching the inlet the absorber. The following condition was imposed at the inlet,

$$q''_{cond}\Big)_{x=0} = -k_s\frac{\partial\langle\overline{T}_s\rangle^i}{\partial x} = q''_{rad}\Big)_{x=0} = \sigma\,\varepsilon_{inl}\,(T_B^4 - T_{env}^4) \tag{10}$$

where σ is the Stephan-Bostzman constant, ε_{inl} is the emissivity of the porous surface, which is here assumed to be a black-body surface for simplicity. Temperature T_B is the solid temperature at the inlet, which is not known and needs to be determined via an iterative procedure. For that, when Equation (10) is discretized using the notation of Figure 1*c*, the following equation is obtained,

$$T_B - T_s = \sigma\frac{\delta\eta}{k_s}(T_{env}^4 - T_B^4) \tag{11}$$

or

$$T_B + \sigma\frac{\delta\eta}{k_s}T_B^4 = T_s + \sigma\frac{\delta\eta}{k_s}T_{env}^4 \tag{12}$$

giving further,

$$T_B(1 + \sigma\frac{\delta\eta}{k_s}T_B^3) = T_s + \sigma\frac{\delta\eta}{k_s}T_{env}^4 \tag{13}$$

that, rearranged, finally gives,

$$T_B = \frac{T_s + \sigma \dfrac{\delta\eta}{k_s} T_{env}^4}{1 + \sigma \dfrac{\delta\eta}{k_s} \left(T_B^3\right)^o} \tag{14}$$

In Equation (14), the superscript "o" on the right-hand-side means value at "old" iterative level. During the iterative process small changes in temperature to the 4th or 3rd power on the right hand side of Equation (14) may lead to numerical instabilities. To avoid that, newly calculated values for boundary temperatures T_B are further relaxed with the help the parameter α_B, such that,

$$T_B = T_B^o + \alpha_B (T_B - T_B^o) \tag{15}$$

where, again, superscript "o" denotes values at the previous iterative level.

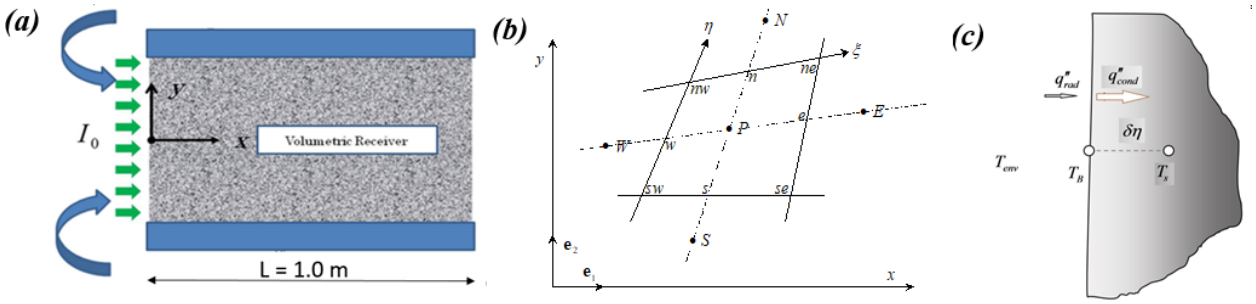

Figure 1 – Problem under consideration and numerical treatment: *a)* Schematic of the solar volumetric receiver, *b)* computational molecule, *c)* radiation boundary condition.

2. RESULTS AND DISCUSSION

Code validation

As mentioned, the procedure for code validation and simulations employed here are the same used elsewhere, or say, computations are compared with reported analytical (Sano *et al.*, 2012) and numerical data (Smirnova *et al.* 2010). The results herein agree well with reported analytical and numerical simulations, ultimately indicating the correctness and accuracy of the developed code.

Mesh independency studies

In order to investigate independency of mesh size on the results, calculations made use of three different two-dimensional grids of sizes 26x110, 52X202 and 114x450 nodes, respectively. After running cases with these three grid sizes, further grid refinement shows that the results become independent of number of nodes. As such, and for conciliating adequate numerical accuracy and reasonable computational cost, all results presented herein were run with a mesh size of 52x202 and the convergence criterion for all variable was set to 10^{-9}.

Solid – Air temperature distribution

For the solid-air temperature distribution in the absorber, Table 1 identifies all cases simulated to obtain of the results. Parameters varied were the porosity ϕ and permeability K. Results to follow show the effect of varying such parameters on both temperature fields.

Table 1 – Cases simulated and respective parameters used.

Cases Investigated	D_p [m]	ϕ	K [m^2]	$Da = K/L^2$
Validation, **Erro! Fonte de referência não encontrada.** and **Erro! Fonte de referência não encontrada.** respectively.	0.0015	0.50	$0.7812\ 10^{-8}$	$0.7812\ 10^{-8}$

Effect of ϕ, on temperatures distribution in the fluid and solid, k_s / k_f =1150	$9.5x10^{-4}$	0.3	$0.3453\ 10^{-9}$	$0.3453\ 10^{-9}$
		0.5	$0.3134\ 10^{-8}$	$0.3134\ 10^{-8}$
		0.7	$0.2389\ 10^{-7}$	$0.2389\ 10^{-7}$
		0.9	$0.4569\ 10^{-6}$	$0.4569\ 10^{-6}$
Effect of ϕ, on temperatures distribution in the fluid and solid, k_s / k_f =2300		0.3	$0.3453\ 10^{-9}$	$0.3453\ 10^{-9}$
		0.5	$0.3134\ 10^{-8}$	$0.3134\ 10^{-8}$
		0.7	$0.2389\ 10^{-7}$	$0.2389\ 10^{-7}$
		0.9	$0.4569\ 10^{-6}$	$0.4569\ 10^{-6}$
Effect of ϕ, on temperatures distribution in the fluid and solid, k_s / k_f =5600		0.3	$0.3453\ 10^{-9}$	$0.3453\ 10^{-9}$
		0.5	$0.3134\ 10^{-8}$	$0.3134\ 10^{-8}$
		0.7	$0.2389\ 10^{-7}$	$0.2389\ 10^{-7}$
		0.9	$0.4569\ 10^{-6}$	$0.4569\ 10^{-6}$
Effect of *Darcy Number* on temperatures distribution in the fluid and solid, k_s / k_f =3500	$7.5x10^{-4}$	0.30	$0.2152\ 10^{-9}$	$0.2152\ 10^{-9}$
	$8.5x10^{-4}$		$0.2765\ 10^{-9}$	$0.2765\ 10^{-9}$
	$9.5x10^{-4}$		$0.3453\ 10^{-9}$	$0.3453\ 10^{-9}$
	$1.5x10^{-3}$		$0.8610\ 10^{-9}$	$0.8610\ 10^{-9}$
	$2.5x10^{-3}$		$0.2392\ 10^{-8}$	$0.2392\ 10^{-8}$

Effect of porosity ϕ

The effect of porosity on the temperature distribution what is plotted as functions of length along the air flow directions. Five porosities, ϕ= 0.3, 0.5, 0.6, 0.7, 0.9 are studied. Kept constant u_{in}=0.7 and D_p=$9.5x10^{-4}$ m, and with thermal conductivity ratio k_s / k_f =5600, there is a decrease in the temperatures profiles as increase the porosity. In the Table 1 it is observed that more efficient porosity is 0.3.

Effect of mean particle diameter D_p

The Figure 2 presents the air and solid temperatures profiles with differents Darcy number. Kept constant ϕ=0.3 and u_{in}=0.7, already the thermal conductivity ratio was set to k_s / k_f =3500. Five Darcy Number, Da = $0.2152\ 10^{-09}$, $0.2765\ 10^{-09}$, $0.3453\ 10^{-09}$, $0.8610\ 10^{-09}$, $0.2392\ 10^{-08}$, are investigated, as previously mentioned, the Figure 3 shows that the decrease in the *Darcy number* favored an improvement in the heat transfer to the fluid, reaching equilibrium temperature more quickly has a significant influence on the temperature distribution of the thermal non-equilibrium region. Shows that the mean particle diameter has a significant influence on the temperature distribution of the thermal non-equilibrium region. For example, when the particle diameter varies from $7.5x10^{-4}$ to $2.5x10^{-3}$, the maximum temperatures of solid phase increases from 1340 K to 1420 K respectively and the similar results were reported by Wang *et al.* (2013).

Finally, the results obtained in this item, as well as in the previous one, follow a trend line similar to those obtained by Wu et al. (2010), and we can see the effect of particle diameter D_p in the *Darcy Number*, decrease in D_p also causes the decrease of *Darcy Number*.

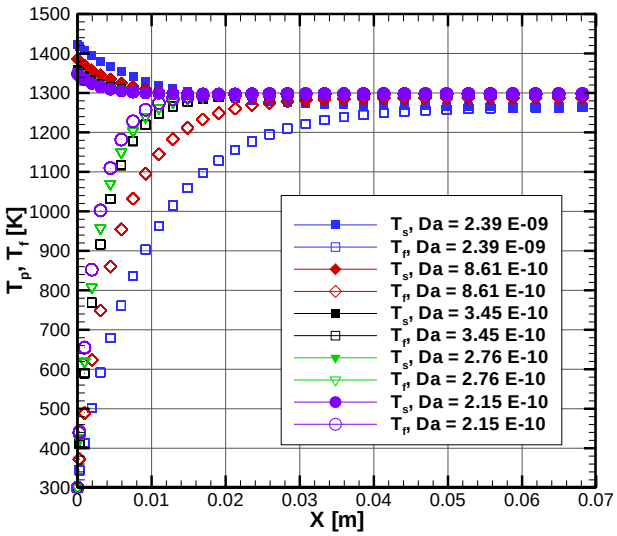

Figure 4 – Axial developments of the air and solid temperature profiles inside an absorber, effect of Darcy Number on on air (T_f) and solid (T_p) temperatures, for ϕ = 0.3, k_s/k_f =3500, inlet velocity u_{in}=0.7 m/s, varying D_p from 7.5x10^{-4} to 2.5x10^{-3} m .

3. CONCLUDIG REMARKS

The analysis of a solar volumetric receiver was investigated using the thermal non-equilibrium hypothesis and radiation boundary condition. The results were compared to analytical and numerical data by (Sano *et al.*, 2012; Smirnova *et al.*, 2010) indicating that temperatures values agreed with the comparisons measurements, It is also possible to conclude that the pressure drops in the absorber agree satisfactorily with the experimental data reported by Wu *et al* (2010). Effects of porosity, mean particle diameter and thermal conductivity ratio k_s / k_f , on the air and solid temperature distribution, were investigated. Increasing k_s / k_f in the absorber material, Implies an increase in the distribution of temperatures, for all cases analyzed. The maximum temperature of solid phase and equilibrium temperature decrease with the increasing of inlet velocity. Also, the maximum temperature of solid phase increases with the particle diameter increasing.

4. ACKNOWLEDGMENTS

The authors are thankful to CAPES, Brazil, for their invaluable support during the course of this research during his tenure at LCFT/ITA.

5. REFERENCES

1. Kreider, J.F.; kreith, F. Solar Heating and Cooling, 2ed. McGraw Hill, USA, 1982.
2. Omar Behar.; Abdallah Khellaf.; Kamal Mohammedi. A review of studies on central receiver solar termal power plants. Renewable and Sustainable Energy Reviews. V.23, p.12–39, 2013.
3. Roldán, M.I.; Fernandez Reche, J.; Ballestrín, J. Computational fluid dynamics evaluation of the operating conditions for a volumetric receiver installed in a solar tower. Energy. V. 94, p. 844-856, 2016.
4. Liao, Z.; Li, X.; Xu,C.; Chan, C.; Wang, Z. Allowable flux density on solar central receiver. Energy. V. 62, p.747-753, 2014.
5. Hendricks, T.J., Howell, J. R. Absorptions scattering coefficients and scattering phase functions in reticulated porous ceramic, Journal of Heat Transfers, v. 118, n.1, p.79-87, 1996.

6. F. Kuwahara, F., Shirota, M. and Nakayama, A., 2001. A numerical study of interfacial convective heat transfer coefficient in two-energy equation model for convection in porous media, Int. Journal Heat Mass Transfer, 44, 1153-1159.

7. Aichmayer, L. Solar Receiver Design and Verification for Small Scale Polygeneration Unit, Master of Science Thesis, Graz University of Technology, Austria, 2011.

8. Bernhard Hoffschmidt.; Félix M. Téllez.; Antonio Valverde.; Jesús Fernández.; Valerio Fernández. Performance Evaluation of the 200-kW HiTRec-II Open Volumetric Air Receiver. Journal of Solar Energy Engineering. V. 125, p.87-94, 2003.

9. Félix M. Téllez Sufrategui. Thermal performance evaluation of the 200kW, SolAir, Volumetric solar receiver. Informes Técnicos Ciemat 1024, Septiembre, 2003.

10. Heller, P.; Pfander, M. ; Denk, T.; Felix, T.; Valverde, A.; Fernandez, J.; Ring, A. Test and evaluation of a solar powered gas turbine system. Solar Energy. V. 80, p.1225–1230, 2006.

11. Fend, T., Pitz-Paal, R., Reutter, O., Bauer, J., Hoffschmidt, B. Two novel high-porosity materials as volumetric receivers for concetrated solar radiation. Sol Energy Mater Sol Cells 2004; 84: 291-304.

12. Wu, Z., Caliot, C., Flamant, G., Wang, Z. Coupled radiation and flow modeling in ceramic foam volumetric solar air receivers. Sol Energy, 2011, 85: 2374-2785.

13. Wu, Z., Caliot, C., Bai, F., Flamant, G., Want, Z., Zhang, J, et al. Experimental and numerical studies of the pressure drop in ceramic foams for volumetric solar receiver applications. Appl Energy, 2010, 87: 504-513.

14. Sano, Y., Iwase, S., Nakayama, A., 2012, A local thermal nonequilibrium analisys of silicon carbide ceramic foam as a solar volumetric receiver, Journal of Solar Energy Engineering, 134(2), 8 pag.

15. Smirnova , O., Fend, T., Schwarzbozl, P., and Schollgen, D., 2010, Homogeneous and Inhomogeneous model for flow and heat transfer in porous materials as high temperature solar air receiver, *Proceedings of the comsol Conference*, Paris, p.17-19.

16. De Lemos, M. J. S. Turbulence in porous media: modeling and applications. 2.ed. Amsterdam: Elsevier, 2012.

17. M.J.S de Lemos, Numerical simulation of turbulent combustion in porous materials. International Communications in Heat and Mass Transfer, **36** (10), p. 996-1001, (2009).

18. M.J.S. de Lemos, Analysis of Turbulent Combustion in Inert Porous Media, International Communications in Heat and Mass Transfer **37** (4), p. 331-336 (2010)

19. M.J.S. de Lemos, Simulation of Turbulent Combustion in Porous Materials with One- and Two-Energy Equation Models, in Heat Transfer in Multi-Phase Materials, Eds: Öchsner, A, Murch, G.E. E., Advanced Structured Materials, Volume 2, p. 443-460, Springer, Heidelberg 2011.

20. M.J.S. de Lemos, Advances in Modeling Turbulence Phenomena in Heterogeneous Media: Reactive Systems. In: Vafai, Kambiz. (Org.). Chapter 13 in: Handbook of Porous Media, Third Edition. Boca Raton: CRC Press - Taylor & Francis, 2015, p. 471-490.

21. Coutinho, J.E.A., de Lemos, M.J.S., Laminar Flow with Combustion in Inert Porous Media, International Communications in Heat and Mass Transfer, v. 39, p. 896-903, 2012.

6. RESPONSIBILITY NOTICE

The Roberta.R.Ribeiro and Marcelo.J.S. de Lemos are the only responsible for the printed material included in this paper.